Diffusion kurtosis imaging of the auditory nerve in unilateral and bilateral deaf patients: An automated processing and analysis pipeline

Christos Tsepas[a]

[a]*Department of Radiology, University Medical Center Utrecht, Utrecht, The Netherlands*

Abstract

Hearing loss is a condition that affects the microstructure of the auditory nerve. Diffusion Kurtosis Imaging (DKI) is a non-invasive MRI technique that can be used to assess the condition of the nerve in patients with hearing impairment. In this study, an automated pipeline for processing and analyzing diffusion-weighted imaging (DWI) data in subjects with normal hearing, unilateral, and bilateral hearing loss is proposed to research any differences in the auditory nerves of these three groups. The pipeline includes preprocessing steps for DWI artefact correction, the application of the DKI model and DTI-based deterministic tractography established on an automated algorithm for region-of-interest (ROI) generation based on manual segmentation of the subjects' cochleae. Qualitative analysis of fiber tract bundle segments revealed alternations in shape and size between the left and right sides. Between normal hearing and unilateral deaf subjects, no significant alternations in the diffusion metrics of either side, for both Phase Encoding directions, were observed. Similarly, no differences were detected when comparing normal hearing and two-sided deaf subjects. Variations in mean kurtosis were investigated to assess the impact of hearing loss on microstructure complexity but with no significant outcomes. The automated pipeline was tested in multiple acquisition sessions in 6 out of 10 subjects and statistically proved to be reproducible. Enhancements to the pipeline can improve the quality of the results and should focus on the correction of deformations caused by EPI distortions and the integration of an automated masking method of the cochleae. Therefore, additional studies with a larger dataset and updated acquisition protocol are needed to validate and expand upon these findings to ensure the acceptance of DKI and fiber tractography as reliable methods for evaluating the condition of the disorder.

Keywords:
Diffusion MRI, Image processing, Fiber tractography, Auditory nerve

1. Introduction

The auditory nerve is an important part of the human auditory pathway that connects the inner ear with the brainstem. Sound waves entering the ear as vibrations, are encoded to electrical impulses by the inner hair cells located inside the cochlea and are transmitted via this nerve to the cochlear nuclei inside the brainstem and other parts of the central auditory nervous system for further processing Møller (2011). The auditory nerve consists of around 31000 to 32000 nerve fibers constructed from bipolar ganglion cells. From these fibers, 90-95% are myelinated type I neurons connecting with the inner hair cells and around 5-10% unmyelinated type II neurons connected to the outer hair cells (Spoendlin (1985), Spoendlin and Schrott (1989)). In people with hearing impairment, a small or total loss of neurons is observed, which strongly depends on the type of degeneration that caused the damage Spoendlin (1975).

Diffusion MRI (dMRI or DWI) is a special MRI technique that can be used to study this nerve. DWI utilizes the 3D Brownian motion of the water molecules inside tissues to extract useful information about their microstructure and connectivity. It is widely used in clinic and research especially for imaging the nervous system Cleveland et al. (1976). Diffusion weighted images are mostly acquired using spin-echo sequence together with Echo Planar Imaging (EPI). Simultaneously, multiple diffusion gradients are applied to both sides of the refocusing (180°) pulse. The gradients have different directions and multiple weightings, whose magnitude is related to the b value (in s/mm^2). The resulting diffusion weighted images are produced with a low signal-to-noise ratio and are prone to artifacts due to subject related and system related reasons, such as the gradient switch, the EPI sequence design and scanner instabilities. These affect the clinical outcomes and increase bias in their qualitative and quantitative evaluation (Baliyan et al. (2016); Tax et al. (2016)). Thus, careful acquisition preparation and further data processing are needed to minimise such artifacts. One of the most challenging parts is the planning of a processing pipeline that takes into consideration all of the artifacts and can correct them in multiple steps before moving to further analysis and quantification of the desired anatomical region Tax et al. (2022).

A major advantage of the DWI is the ability to use the information of how much hindered or free the water diffusion in the tissue is. This can be linked to the structure of the tissue. Changes in this hindrance indicate structure change which can be a result of a pathology Beaulieu (2002). Assuming that water

Email address: c.tsepas@students.uu.nl (Christos Tsepas)

molecules follow Gaussian distribution, the magnitude and the dominant orientation of the motion can be described by a model called diffusion tensor imaging (DTI). DTI can be used to measure the degree of anisotropic diffusion inside the tissue (Basser et al. (1994)) and to quantify this anisotropy with metrics like fractional anisotropy (FA) and mean diffusivity (MD). Pathology causes damage in the tissue and affects the hindrance of the water resulting in changes in the DTI tensor and the aforementioned parameters. The anisotropic diffusion has a principle orientation, which is described by the eigenvectors of the DTI tensor. By the use of computational algorithms, the principal orientation in multiple voxels can be tracked reconstructing artificial neural pathways. Connecting the axons to a streamline, a 3D reconstruction of the neural pathways can be performed with a technique called fiber tractography Basser et al. (2000). Fiber tracking is a well-known method in brain research and is used for quantification and visualization of tissue architecture.

More complex models, such as the diffusion kurtosis tensor (DKI), can also be used to investigate the diffusion phenomenon. Assuming movement that deviates from Gaussian distribution, the DKI model uses the non-Gaussian order to further describe complex tissues and their grade of structure Jensen et al. (2005). Parameters like Mean kurtosis (MK), Axial kurtosis (AK) and Radial Kurtosis (RK) are used to quantify the degree of kurtosis. In biophysical models due to the tissue's complicated structure, the water diffusion may not follow Gaussian distribution. This deviation described from the kurtosis tensor can be regarded as a measure of a tissue's degree of structure. Thus, both DTI and DKI are suitable models for a non-invasive study of the auditory nerve.

In clinical research, DTI has been used to study the auditory pathways in patients with Congenital Cochlear Nerve Deficiency (CND) Wu et al. (2009) and Unilateral Acoustic Neuroma Kurtcan et al. (2016) in Inferior Colliculus and Lateral Lemniscus, as well as for investigating microstructural alternations related to ageing both in the previous anatomies and Heschl's gyrus Lutz et al. (2007). A significant decrease in FA and an increase in MD have been noticed, verifying that changes in DTI parameters occur in pathological tissue and indicating its advantage over conventional MRI techniques in the diagnosis of auditory diseases. Chinnadurai et al. (2016) used both DKI and DTI models in CND and highlighted the importance of kurtosis parameters in estimating and providing new insights about microstructural differences. In a study of Kim et al. (2020), DTI and DTI based tractography are proposed as possible candidates to access the microstructural changes in subjects with hearing loss. Both of these studies are focused mostly on the brainstem and the cortical auditory pathways. Vos et al. (2015) researched explicitly the auditory nerve using DTI and fiber tractography highlighting some interesting facts. In single sided deaf patients, no significant differences in the FA between healthy and deaf sides were found, but both sides showed significantly reduced FA when compared to normal subjects. They suggested that several things need to be improved for a better study of the region. To name a few, a greater number of subjects, higher resolution of DWI, different acquisition protocols and a more complicated model, such as DKI, could be possible solutions for further research.

In literature, there are multiple generic pipelines to process dMRI data, some of them optimized for the brain. Each anatomy, like the auditory nerve, has its challenges and specifications making the commercial pipelines rather than applicable. Thus, a fully optimized processing pipeline that matches the requirements of this tiny structure needs to be created. Another major concern is that, in the literature, there are only DTI metrics provided for this region of interest in a limited group of subjects and only between normal hearing and one-sided deaf subjects Vos et al. (2015). With a small background information, the quantification of the auditory nerve is uncharted territory.

This study aims to provide an automated and optimized processing and analysis pipeline of dMRI data of normal hearing, single-sided and two-sided deaf patients using the DKI model and DTI-based fiber tractography. Also, it will be tested in multiple sessions of the same subjects to evaluate its reproducibility. As degeneration can cause neuron loss and change in microstructural properties Spoendlin (1975), a hypothesis that there is a difference in DTI and DKI parameters between the auditory nerves of normal hearing subjects and unilateral and bilateral deaf patients will be tested.

2. Materials and Methods

2.1. The DTI and DKI model

The DTI model assumes a Gaussian distribution of the diffusion of water molecules inside the tissues. Given the DWI images and an anatomical T2, the water diffusivity is estimated by the diffusion tensor (**D**). The tensor can be visualized as an 3D ellipsoid defined by given centre and surface coordinates. Its main three orientations are mathematically described by eigenvectors (ϵ_1, ϵ_2, ϵ_3) with magnitudes the eigenvalues (λ_1, λ_2, λ_3). The size of the ellipsoid is related to the distance that a water molecule can travel from its centre to the surface, while its first eigenvector defines the main orientation of the diffusivity Basser et al. (1994). FA and MD can be calculated from the diffusion tensor and used as DTI quantification parameters. MD is estimated by the average of the eigenvalues (Trace(**D**)/3 in mm^2/s) describing the diffusivity of the water molecules in a specific area for a given time, while FA is the degree of anisotropy (values 0 from isotropic to 1 high anisotropic) Basser (1995). MD can take positive values, while white , 0.2-0.4 for grey matter and below 0.2 for CSF. For visualization purposes, RBG colour encoded maps are used for understanding the main orientation of the ellipsoid (Anterior-Posterior → green, Left-Right → red, Superior-Inferior → blue) Pajevic and Pierpaoli (1999).

DKI model assumes a non-Gaussian distribution of the water molecules and describes the displacement of the probability function from its normal distribution (Figure 1 Steven et al. (2014)) as a form of peakedness Balanda and MacGillivray (1988). Given the equation that describes the DTI model:

$$\ln\left(\frac{S(b)}{S_0}\right) = -b\boldsymbol{D} \tag{1}$$

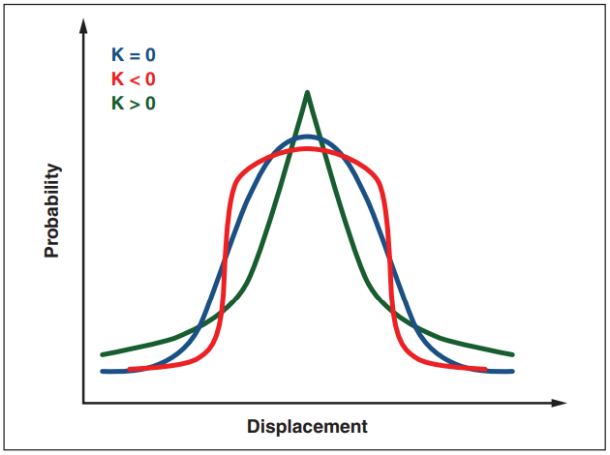

Figure 1: Probability distribution for different kurtosis values. A kurtosis of zero aligns with a Gaussian distribution.

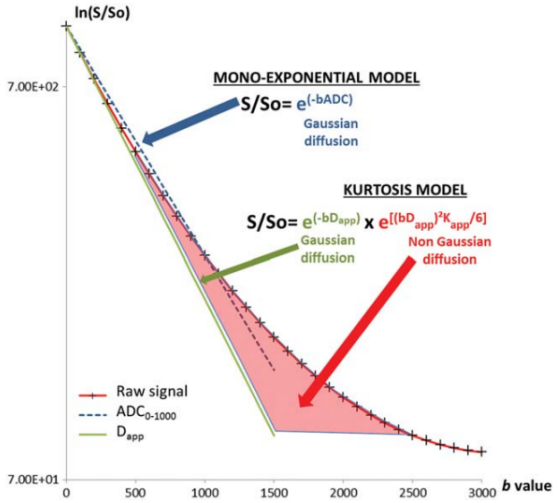

Figure 2: Natural logarithm of the DWI signal attenuation as a function of the b value. The fit of the signal decay using monoexponential (DTI) and DKI model.

the deviation from the Gaussian distribution is described in the DWI signal equation as a second polynomial order

$$\ln\left(\frac{S(b)}{S_0}\right) = -b\boldsymbol{D} + \frac{1}{6}b^2\boldsymbol{D^2K^2} \tag{2}$$

where b_i is the b value, **D** is the diffusion tensor and **K** is the Kurtosis tensor. Kurtosis metrics, like Mean Kurtosis, Axial Kurtosis (AK) and Radial Kurtosis (RK), can be derived to describe the complexity of the structure. In tissues like white matter AK is expected low, while RK is high Steven et al. (2014). From Equation 1, DTI parameters can be estimated from the DKI model too.

For b-values above 1000 s/mm^2, the model estimation of the natural logarithm of the signal decay is no longer linear. The DTI model cannot accurately describe the DWI signal attenuation (figure 2 Rosenkrantz et al. (2015)). Thus, the deviation of the linearity can only be estimated with a more complicated model like DKI. Kurtosis imaging requires multi-shell DWI data with at least 30 gradient orientations and two b-values > 1000 s/mm^2, which results in longer echo times and, subsequently scanning time.

2.2. *Study population and data characteristics*

The group consists of 10 healthy subjects (each scanned 4 times in different sessions), 10 additional healthy volunteers, 9 one-sided and 13 two-sided deaf individuals.

The dataset of each subject contains 2 multi-shell 4D DWI volumes acquired with opposite Phase Encoding directions (Anterior-Posterior, Posterior-Anterior). The diffusion weighted volumes were acquired with b-values of b = 1 s/mm^2(13 gradients), b = 400 s/mm^2(20 gradients), b = 900 s/mm^2(40 gradients) and b = 1500 s/mm^2(60 gradients). The voxel resolution is 1.8 mm^3 isotropic and the image dimensions 128 × 128 × 20. In addition, an axial 3D T2-weighted anatomical volume of voxel resolution 0.25 × 0.25 × 0.50 mm^3 with dimensions 528 × 528 × 50, a sagittal anatomical T2-weighted volume and two survey scans are acquired with the same scanning parameters described in Vos et al. (2015).

2.3. *Image processing*

The DWI data, and especially those with high b-values, have relatively low SNR due to fast echo-planar acquisition methods, the low signal and the presence of thermal noise in the scanner. This has a great impact on the calculation of DWI parameters (such as MD), the DTI tensor estimation and the reconstruction of fiber tracts (Jones and Basser (2004). Thus, denoising was performed on the data using DIPY (Garyfallidis et al. (2014)). The PCA reconstruction was done automatically with random estimation of noise variance based on the Marchenko-Pastur distribution (Veraart et al. (2016)).

The resulting data were masked in DIPY using a median filter smoothing of the input volumes and an automatic histogram Otsu thresholding to eliminate the effect of the background to signal drift estimation. Masking parameters were chosen by trial and error with the main focus on maintaining the anatomy surrounding the auditory nerve. Subsequently, the data were corrected for signal drift between DWI volumes caused by scanner instabilities, like heating, during multiple acquisition series (Vos et al. (2017)). The signal drift was estimated based on b = 400 s/mm^{2}volumes and both the estimation and correction were done on ExploreDTI (Leemans et al. (2009)). The data were sorted from the smaller to bigger b values and cropped to 78 × 50 × 20 eliminating the extensive zero background.

Subject motion and eddy current distortions, caused by the switch of the gradients during acquisition, result in artifacts and increased bias to quantitative parameters, such as the FA Pierpaoli (2010). The DWI volumes were corrected for these artifacts by aligning them to those with b = 1 s/mm^2, which were treated as non-DWI for the further processing steps, with proper rotation of the B-matrix Leemans and Jones (2009). Affine registration was performed with 12 degrees of freedom and linear interpolation using `elastix` Klein et al. (2009).

T2 volumes were resampled to 1.8 mm isotropic voxel resolution with trillinear interpolation on ExploreDTI and extra

anatomies, like the front and rear parts of the skull, were cropped to $72 \times 56 \times 14$ in DIPY to match the FOV of the DWI data. Negative pixel values resulting from resampling were set to 0. The volumes were rigidly aligned to the average of b=1 s/mm^{2}volumes.

In the last step, the DTI and DKI model were fitted on the DWI data using the REKINDLE estimation Tax et al. (2015) in native space.

2.4. Tractography

Whole brain DTI-based deterministic streamline tractography was performed to AP and PA datasets for each subject. Seed point resolution was set to 1 mm^3 and the FA threshold for seeding to 0.04, which is low as the auditory nerve pathway is influenced by partial volume effect from the CSF Vos et al. (2011, 2015). FA and MD tracking thresholds range from [0.01, 0.9] and [0.0002, 0.01] mm^2/s, respectively. Fiber tracts with length [10, 500] mm with a maximum angular resolution of 20° were allowed. The tractography was conducted with a step size of 0.5 using linear interpolation.

Taking into account the tiny structure of the auditory nerve, the cochleae were used as Seed for tractography analysis. Each cochlea was manually outlined and segmented as a 3D cube (of approximately from 278 to 370 mm^3, depending on the size) on ITK-Snap (Yushkevich et al. (2006), www.itksnap.org) based on the aligned T2-weighted images and the average b = 1 s/mm^{2}DWI volumes, except in a small those subjects or sessions whose anatomical image was missing. The binary masks are stored separately for the left and right cochlea for each subject. The coordinates of the centre point were defined and used as parameters to create 3D hexagonal Seed ROIs that outline the region of the cochleae. Based on the two center coordinates, the mid-point was calculated as half of their distance and the mid-sagittal plane was defined for each subject. The mid-point was transformed to the right and left 75% its distance from the right cochlea as

$$x_R = x_0 + 0.75\times \mid x_{(cochlea)_R} - x_0) \mid \tag{3}$$

and left cochlea

$$x_L = x_0 - 0.75\times \mid x_{(cochlea)_L} - x_0) \mid \tag{4}$$

respectively.

In this way, the sagittal plane transformation depends on the anatomy and the distance of each subject's cochleae from the brain stem. The reason for choosing this method is that is more robust to anatomical changes in the subject's brain size and shape. From the transformed plane, a rectangular ROI will be created and used as a terminating point for the tractography. For automation purposes, and to match each subject's specific characteristics, the corners of the rectangular depend on the minimum and maximum y,z coordinates of the hexagonal Seed ROI. The rectangular extends 2 voxels below and 1 voxel above the z_{min} and z_{max} on the z plane, while 4 voxels below and 2 voxels above the y_{min} and y_{max} respectively. By reducing the size of the terminating ROIs, false tracts are excluded,

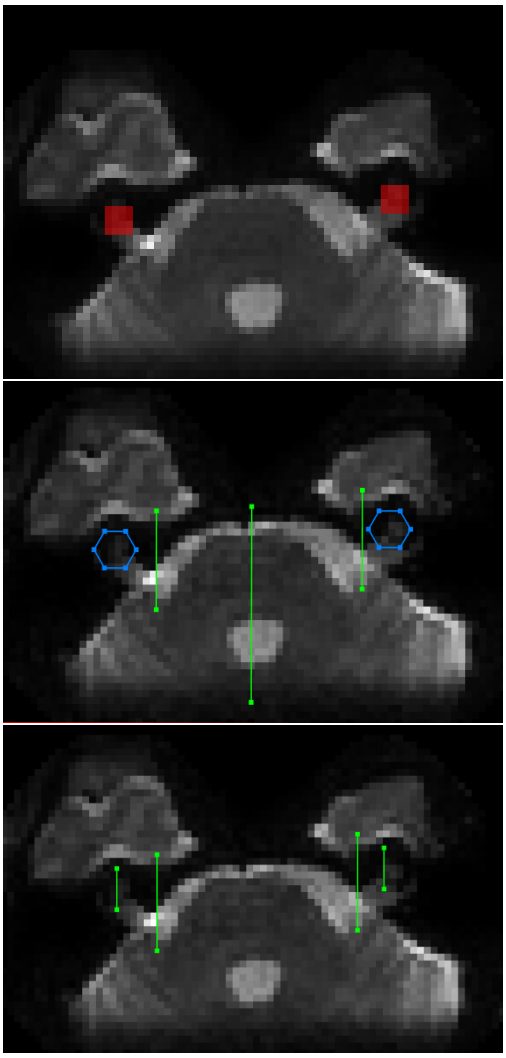

Figure 3: Manual cochleae segmentation used as an input for the automated ROI generation algorithm (first figure). Hexagonal seed and rectangular ROIs used for tractography analysis (second above) and segmentation (third figure). The big green ROI represents the mid sagittal plane between the two cochleae.

aiming at the localization of the auditory nerve. This is very important, especially when dealing with a large dataset, where the visualization and analysis of each subject's tracts individually is time-consuming. This automated method is heavily influenced by the quality of the input masks of the segmented cochleae. For the segmentation of the auditory nerve tracts, another rectangular ROI is located 1 voxel ahead of the centre of the Seed ROI with the same length and width as the hexagon (Figure 3).

Thus, an automated method was created for analysing and segmenting the auditory nerve tracts. For a matter of simplicity, a Python interface with all the processing steps was created. The user can type the processing step that wants to do and specify the input and output paths except for the steps that require the ExploreDTI toolbox. Regarding the tractography analysis, the user can specify the input and output path in the Matlab scripts, but with the ExploreDTI GUI running in the background. The scripts for both the processing pipeline and the tractography analysis as well as a file with a detailed

Table 1: Diffusion tensor and kurtosis measures per group (mean (standard deviation) over subjects within the group) of the AP data.

	Subject Groups (AP)		
	Normal hearing	**Single-sided deaf**	**Two-sided deaf**
FA			
Left	0.16 (0.03)	0.15 (0.02)	0.16 (0.03)
Right	0.18 (0.04)	0.18 (0.01)	0.17 (0.03)
MD (10^{-3} mm^2/s)			
Left	2.21 (0.43)	2.47 (0.18)	2.11 (0.48)
Right	2.26 (0.43)	2.39 (0.29)	2.54 (0.50)
MK			
Left	1.40 (0.75)	1.22 (0.11)	1.51 (0.54)
Right	1.14 (0.60)	1.20 (0.29)	1.09 (0.43)
AK			
Left	1.29 (0.54)	1.10 (0.10)	1.34 (0.40)
Right	1.13 (0.38)	1.07 (0.21)	0.98 (0.34)
RK			
Left	1.52 (0.84)	1.25 (0.14)	1.57 (0.65)
Right	1.21 (0.55)	1.26 (0.34)	1.13 (0.48)

Table 2: Diffusion tensor and kurtosis measures per group (mean (standard deviation) over subjects within the group) of the PA data.

	Subject Groups (PA)		
	Normal hearing	**Unilateral deaf**	**Bilateral deaf**
FA			
Left	0.21 (0.03)	0.17 (0.02)	0.19 (0.03)
Right	0.19 (0.04)	0.20 (0.05)	0.19 (0.03)
MD (10^{-3} mm^2/s)			
Left	1.94 (0.43)	2.27 (0.18)	1.96 (0.41)
Right	2.14 (0.34)	2.03 (0.37)	2.04 (0.37)
MK			
Left	1.51 (1.03)	1.14 (0.29)	1.59 (0.47)
Right	1.43 (0.48)	1.64 (0.48)	1.55 (0.46)
AK			
Left	1.45 (0.73)	1.04 (0.23)	1.52 (0.58)
Right	1.28 (0.38)	1.42 (0.37)	1.39 (0.37)
RK			
Left	1.63 (0.99)	1.13 (0.33)	1.24 (1.10)
Right	1.41 (0.54)	1.68 (0.53)	1.52 (0.55)

description of the algorithms and the code can be found at `https://github.com/ChristosTsepas/Major-Project`.

2.5. Statistical analyses

Group analysis and statistical tests were performed on Microsoft Excel. First, to evaluate the reproducibility of the whole processing and analysis pipeline, differences in mean FA across subjects of the same session are investigated using the ANOVA test. Each session across subjects represents a group and the variability between the 4 groups is tested. A two-tailed paired t-test was applied to compare FA, MD, MK, AK and RK between the left and right auditory nerve tract. Data of opposite Phase-Encoding directions are treated as different datasets. In the last step, the dataset was divided into three groups, normal hearing, one-sided and two-sided deaf subjects. Between groups, F-tests were performed to investigate if there were differences in the variances. Depending on the results of the F-tests, two sampled t-tests (with or without equal variances) were performed between normal-hearing and one-sided deaf as well as normal-hearing and two-sided deaf individuals. The main focus is to detect any significant alternation in the diffusion parameters between groups.

3. Results

3.1. Processing

From the single-sided group, 5 out of 9 groups were used to the whole processing pipeline because 3 subjects didn't have a clear indication of the PE direction (AP or PA) and subject 8 had fewer DWI volumes than 133. Also, some sessions from normal hearing subjects were excluded due to the lack of axial anatomical T2 volume, missing volumes or due to missing data of opposite PE direction. From the raw data, 126 datasets were used for processing. Results of the automated algorithm used for tractography analysis and segmentation show that 121 out of 125 left tracts (96.8%) and 107 out of 125 right tracts (85.5%) could be reproduced and reconstructed. One session from the normal hearing subject 10 was excluded for both AP and PA datasets as it were corrupted files. From the resulting segmentations, 9 left tract and 4 right tract segments showed very high negative Mean Kurtosis values. 8 out of 9 left and 4 right were manually resegmented to reduce false positive tracts. The rest of the tracts that couldn't be reconstructed were manually evaluated and segmented respecting the already generated ROIs from the algorithm.

3.2. Tract segment analysis

Opposite PE data were split into two sub-datasets as they showed significant qualitative differences and couldn't be concatenated into a single dataset. The following analysis was performed on AP and PA datasets independently.

3.2.1. Reproducibility

The reproducibility was tested separately for left and right tracts. For the ANOVA tests subjects whose tracts could be reconstructed for every session are included. For the AP data, 6 subjects were used for both left ($F = 1.27$, $F_{crit} = 3.10$, $p = 0.31$) and right tracts ($F = 0.40$, $F_{crit} = 3.13$, $p = 0.76$). For the PA data, 6 subjects were used for left ($F = 0.75$, $F_{crit} = 3.22$, $p = 0.53$) and right ($F = 0.24$, $F_{crit} = 3.00$, $p = 0.87$). For the percentage of the data used for the statistical test, the results showed reproducibility of the analysis for both left and right tracts. The second session for each subject used for the ANOVA test was included in the dataset for the following analysis.

Table 3: Results of paired t-tests between left and right side for AP data.

	p-value (AP)		
	Normal hearing	**Unilateral deaf**	**Bilateral deaf**
FA	0.12	0.09	0.54
MD	0.70	0.50	0.03
MK	0.26	0.86	0.09
AK	0.33	0.75	0.28
RK	0.24	0.94	0.12

Table 4: Results of paired t-tests between left and right side for PA data.

	p-value (PA)		
	Normal hearing	**Unilateral deaf**	**Bilateral deaf**
FA	0.15	0.33	0.56
MD	0.20	0.30	0.47
MK	0.84	0.196	0.75
AK	0.48	0.199	0.42
RK	0.55	0.197	0.55

3.2.2. Fiber bundle segment

Qualitatively, a notable discrepancy in the number of tracts between the left and right segments can be detected. The mean length of the whole dataset is 9.5 mm for the left and 12.8 mm for the right segments, almost two voxels difference. In addition, a few false positive tracts are included in the segments, which correspond to tracts from remaining artefacts (or noise) after the preprocessing pipeline as well as tracts due to EPI deformations (Figure 4). The automated algorithm for ROI generation plays a crucial role as the size and shape of the generated ROIs cannot exclude tracts that are unrelated to the auditory nerve.

Mean values of diffusion parameters per group can be found in tables 1 6. Overall, lower FA and higher MD are estimated in the subject groups compared to controls, except for the MD values of the right side in PA data. Regarding the DKI parameters, MK becomes smaller in the patient groups, but only in the AP data. For AK and RK, no clear pattern in the values is found. Also, the difference between the two sides in each group is profound. A detailed description of the inter-subject variability can be found in figure 5.

No laterality differences were noticed between left and right tracts for all diffusion parameters. Only the mean MD in two-sided deaf (AP) showed significant differences between the left and right sides, but this might be mostly due to the high standard deviation per subject and the nature of the data (false tracts) and not the means themselves.

As no significant differences were found in the normal hearing subjects, the left and right tracts per subject were averaged and used for the next statistical step. Comparing the normal hearing and unilateral deaf groups, the only decrease, slightly above the approved value for statistical significance, was noticed on the mean FA of the left side for PA data (FA: p = 0.06). For the left side of the AP data mean FA showed a decrease with (FA: p = 0.08), but cannot be accepted. No significant alternations were observed in the other diffusion metrics. Comparing normal hearing and bilateral deaf subjects, no significant differences were found. No statistically accurate differences in diffusion metrics were observed even when comparing the two patient groups.

Table 5: Results of the t-test comparing average normal hearing and one-sided and two-sided deaf.

	p-value (AP)	
	NH vs Unilateral deaf	**NH vs Bilateral deaf**
FA		
Left	0.08	0.34
Right	0.74	0.84
MD		
Left	0.18	0.47
Right	0.39	0.09
MK		
Left	0.75	0.30
Right	0.79	0.40
AK		
Left	0.31	0.41
Right	0.43	0.12
RK		
Left	0.46	0.40
Right	0.64	0.28

4. Discussion

In this report, an automated pipeline for processing and analysing DWI data of three subject groups (normal hearing, unilateral and bilateral deaf) is proposed. DTI-based deterministic tractography was performed on the processed data and an automated algorithm for automated ROI generation for tractography analysis based on manual segmentation of the cochleae is suggested. Albeit the resulting left and right side tracts showed alternations in their shape and number, there was no difference in the mean value of the DTI and DKI parameters between the two sides of each group's subjects. Normal hearing and one-side deaf group comparison showed a lower mean FA in the left tracts of the patient group for PA data. On the other hand, lower FA and higher MD were observed between controls and bilateral deaf subjects only for the right side of the AP data, but with no significance. The results tend to show the expected behaviour for FA and MD between controls and patients, but the high standard deviation within the group cannot ensure that the FA, indeed, decreases and MD increases in the patients. Lower FA is an indication of demyelination in the structure of interest and the results justify this as both of the patient groups showed a decrease. The same with MD, where increased diffusivity is connected with less hindrance in the water diffusion and higher water content in the tissue Hetherington et al. (2015), which might be the result of inflammation that caused the hearing loss in the subjects Eisenhut et al. (2019). The partial volume effects are dominant and present in the calculation of mean FA, whose

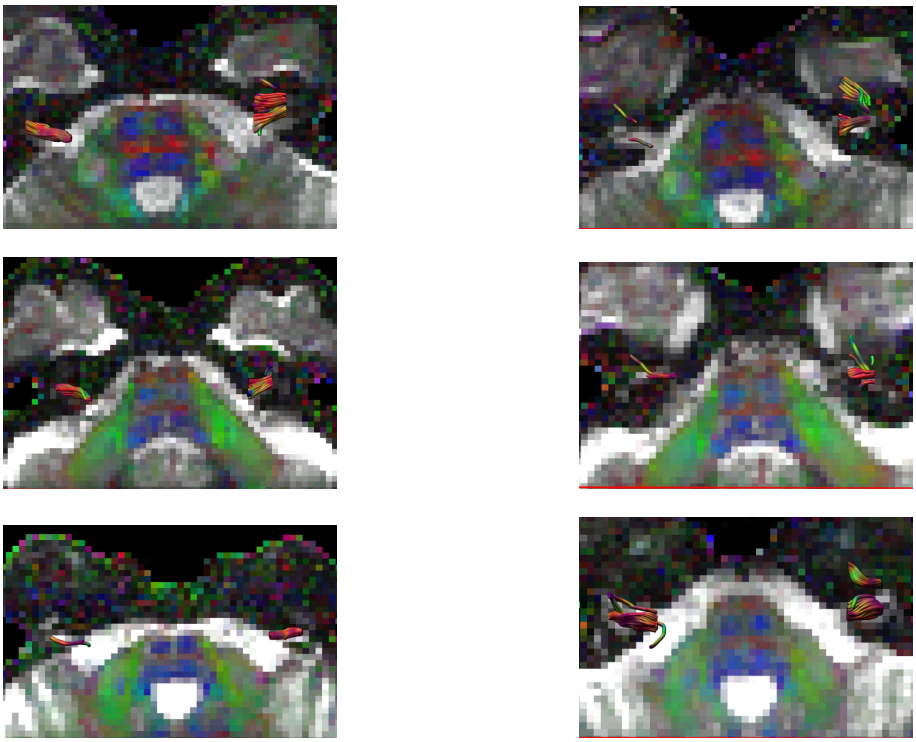

Figure 4: Qualitative tractography results of 3 random subjects representing each group (normal hearing, single-sided and two-sided deaf subjects). At each row, AP (left) and PA (right) data are depicted. The tracts are visualized on top of the first b=1 s/mm^{2}volume together with directional encoded colour maps. Profound differences in the anatomical features and the number of true and false positive tracts between the opposite PE volumes can be noticed.

Table 6: Results of the t-test comparing average normal hearing and one-sided and two-sided deaf.

	p-value (PA)	
	NH vs Unilateral deaf	**NH vs Bilateral deaf**
FA		
Left	0.06	0.34
Right	0.97	0.54
MD		
Left	0.09	0.70
Right	0.98	0.90
MK		
Left	0.21	0.68
Right	0.65	0.82
AK		
Left	0.08	0.57
Right	0.90	0.99
RK		
Left	0.07	0.44
Right	0.67	0.88

values are closer to those of the CSF rather than white matter. Although changes in DTI parameters are observed, the initial hypothesis cannot be accepted either in unilateral deaf subjects or the bilateral deaf group. Information on the tissue type and complexity can be derived from the DKI parameters. Positive MK indicates a complex structure within the region of interest, which affects the water diffusion and its Gaussian behaviour. The distribution of the MK values don't provide essential information to understand whether the disorder alters the complexity of the tissue's microstructure. AK proved to be smaller than RK, which as of Steven et al. (2014), is an indicator that the segmented tracts contain anatomy with myelinated fibers, but with a huge influence from partial volumes. Comparing the results with previous work of Vos et al. (2015), both mean FA and mean MD appeared higher. For the former, this happened due to the way the fiber tracts were segmented (less accurate when compared to manual segmentations), while the latter is because of the different fitting of the DKI model to the signal decay. However, to have a clear indication of the distribution of the results, the whole dataset needs to be included and statistical analyses to be performed in the total batch. The exclusion of some datasets affects the outcomes.

4.1. Limitations

In quantification MRI, errors occurred throughout the whole pipeline propagate and have negative effects on the results. It is crucial to optimize and validate each step of the pipeline, from the processing steps to the model, as well as the nature of the data. Understanding the limitations of the study can lead to possible solutions to these negative effects.

4.1.1. Processing pipeline

Even though the data of the same subject represent the same anatomy, the AP and PA data have strong dependencies on the PE direction during the acquisition. This can be noticed both qualitatively, by looking at the images, and quantitatively, on

Figure 5: Box plots of the mean of the diffusion parameters of all points of all tracts in fiber bundle segment per subject. On the left the AP data with population N_1=5, N_2=11 and N_3=15 per side, for normal hearing, unilateral and bilateral deaf subjects with their code names respectively. On the right, the PA data with population N_1=5, N_2=10 and N_3=15 per side, accordingly.

the inconsistent mean values of the diffusion parameters. Both the cochlea and the auditory nerve are heavily deformed due to susceptibility-induced Echo Planar Imaging distortions Vos et al. (2015); Jezzard and Balaban (1995). The reason for acquiring data with opposite PE directions was for the correction of such deformations, something that the pipeline considered not to take into account with the data remaining in native (DWI) space. Experiments were conducted on ExploreDTI, especially non-rigidly aligning each subject's data to the respecting T2 volumes to eliminate these artefacts. The outcomes were far from satisfactory as the AP and PA dependencies were still present and the opposite PE data couldn't be concatenated into a single dataset. Also, deformations and blurring were noticed when transforming the DWI volumes to the T2 space and the resulting tracts did not align with the expected anatomical region where the auditory nerve should have been located. Further research needs to be done for the correction of these artefacts and focus mostly on the optimization of the registration procedure. Both FSL and elastix (called internally from ExploreDTI) were used with no clear indicator of the optimal software for correcting the deformations. The optimization needs to be localized on the region around the cochlea and the auditory nerve and tools validating on whole brain volumes might not be the suitable candidate. Another possible solution is to use DIPY's Symmetric Diffeomorphic Registration in 3D. First, the deformation field can be estimated by non-rigidly aligning the DWI data to the T2 volume and then the deformation field will be applied again to the DWI volumes to correct for EPI distortions. This idea is in between what FSL and ExploreDTI do. Another idea is to develop a new registration algorithm which calls internally the elastix toolbox and can be carefully optimized on the cochlea and auditory nerve.

Regarding the automated pipeline, future improvements will focus on making it more user-friendly. The user can already specify the processing step and folder path, but some of the parameters used in specific functions are predetermined. In future releases, the user will be able to specify parameters, like image dimensions on cropping, dilation in masking and patch radius in denoising, from the interface without diving into the scripts. Also, the aim is to avoid changing programming languages and interfering with the Matlab scripts for ROI generation and tractography analysis. Work will be conducted for the scripts to be called internally using the Matlab engine for Python.

4.1.2. Tractography analysis

The automated algorithm for ROI generation and tractography analysis is based on validated APIs like ExploreDTI and Python's Numpy library. It was designed in a way that it can reduce systematic errors as much as possible and limit user interference only on the manual segmentations and the specification of ROI size and shape. Thus, any error occurring in the analysis is based on these two factors. The uneven tract length testifies to the existence of the algorithm's limitations. The transition from voxel coordinates to world coordinates as well as from Numpy to Matlab and ExploreDTI GUI's interpretation of data caused voxel shifting. Also, miscalculation of midpoint coordinates exists due to uneven cochleae. The midpoint is determined based on the centre coordinates of the masks, but if the masks are not on the same x-line the sagittal plane perpendicular to the midpoint will be determined with a voxel difference. Even though these points need improvement, such a difference in the tract length couldn't make so much difference in the calculation of the diffusion parameters. On the other hand, this could justify why fewer tracts were produced on the right side of the subjects. To eliminate the false negative tracts the ROIs used for segmentation can be smaller and more precise on the actual location of the tracts. The automated algorithm can take advantage of the information provided on tract density maps to create ROIs that match the tract's size and shape. Regarding the masking, semi-automated methods like the one proposed on Matloff et al. (2021), can be used as an alternative to manual segmentation of the cochleae. The method is based on T2-weighted images, so to be implemented properly, the successful elimination of EPI deformations and alignment with the T2 volume is required. These improvements can eliminate systematic errors and enhance the robustness of the method.

4.1.3. Image acquisition

Even though the main focus is on data processing, some improvements for data acquisition can be suggested. Taking into account the small cross-section of the auditory nerve (around 0.5 mm) acquisition protocol needs to be designed with a smaller voxel size (even lower than 1 mm^3). High resolution will help distinguish the auditory nerve from its counterpart, the vestibular nerve, and the surrounding CSF. The need for larger resolution can be noticed in the provided data too. By observing the data acquired with 1.8 mm^3 resolution, one can see that the area surrounding the auditory nerve consists of a few voxels (sometimes even 2 or 3). This, also, makes it difficult for the tractography analysis as there is a hit-or-miss chance of not losing the voxel that contains the important information, especially when motion artefacts occur. Another suggestion would be the acquisition of volumes with at least an extra b-value > 1000 s/mm^2 (i.e. 2000 s/mm^2). Acquiring volumes with at least two b values above 1000 s/mm^2 would be beneficial to the tensor fitting as it will add more weights to a more precise estimation of the diffusion parameters. With higher resolution and increase of the diffusion gradients, larger scanning times are needed and the resulting images might be prone to thermal noise and artefacts due to subject motion. Thus, a realistic acquisition protocol needs a balanced design that carefully considers the voxel resolution, time and limitation of such artefacts.

For further investigation of the auditory pathways beyond the auditory nerve the acquired data must include parts of the brain up until or above the temporal lobe. By increasing the FOV, the same techniques and principles can be applied to examine and investigate any differences in areas like the inferior colliculus, lateral lemniscus and the primary and secondary auditory cortex in patients with hearing loss.

5. Conclusion

In this study, an automated pipeline for processing and analysing DWI data of healthy, one-sided and two-sided deaf

subjects is proposed. No laterality differences were found between the subjects' left and right tracts and no significant reduction was noticed in the diffusion metrics of both unilateral and bilateral deaf patients. Further research needs to be done to confirm that the DKI model can be used to access patients with hearing loss. Therefore, the hypothesis cannot be accepted as the results lack universality and are not verified for the patient groups of this study.

Acknowledgements

I would like to thank my supervisor, dr.ir.Martijn Froeling, for his invaluable guidance and support throughout this project. His expertise and insightful advice have been crucial in introducing me to the challenging field of diffusion MRI data processing and fiber tractography as well as shaping my direction in research. Additionally, I would like to thank dr.Alberto De Luca for our discussions and his insights regarding topics in diffusion MRI processing and the functionality of the ExploreDTI toolbox. Their contributions were very important in accomplishing my research goals and overcoming challenges that came up throughout the project.

References

Balanda, K.P., MacGillivray, H., 1988. Kurtosis: a critical review. The American Statistician 42, 111–119.

Baliyan, V., Das, C.J., Sharma, R., Gupta, A.K., 2016. Diffusion weighted imaging: technique and applications. World journal of radiology 8, 785.

Basser, P.J., 1995. Inferring microstructural features and the physiological state of tissues from diffusion-weighted images. NMR in Biomedicine 8, 333–344.

Basser, P.J., Mattiello, J., LeBihan, D., 1994. Mr diffusion tensor spectroscopy and imaging. Biophysical journal 66, 259–267.

Basser, P.J., Pajevic, S., Pierpaoli, C., Duda, J., Aldroubi, A., 2000. In vivo fiber tractography using dt-mri data. Magnetic resonance in medicine 44, 625–632.

Beaulieu, C., 2002. The basis of anisotropic water diffusion in the nervous system–a technical review. NMR in Biomedicine: An International Journal Devoted to the Development and Application of Magnetic Resonance In Vivo 15, 435–455.

Chinnadurai, V., Sreedhar, C., Khushu, S., 2016. Assessment of cochlear nerve deficiency and its effect on normal maturation of auditory tract by diffusion kurtosis imaging and diffusion tensor imaging: A correlational approach. Magnetic Resonance Imaging 34, 1305–1313.

Cleveland, G., Chang, D., Hazlewood, C., Rorschach, H., 1976. Nuclear magnetic resonance measurement of skeletal muscle: anisotrophy of the diffusion coefficient of the intracellular water. Biophysical journal 16, 1043–1053.

Eisenhut, M., et al., 2019. Evidence supporting the hypothesis that inflammation-induced vasospasm is involved in the pathogenesis of acquired sensorineural hearing loss. International Journal of Otolaryngology 2019.

Garyfallidis, E., Brett, M., Amirbekian, B., Rokem, A., Van Der Walt, S., Descoteaux, M., Nimmo-Smith, I., Contributors, D., 2014. Dipy, a library for the analysis of diffusion mri data. Frontiers in neuroinformatics 8, 8.

Hetherington, H., Bandak, A., Ling, G., Bandak, F., 2015. Advances in imaging explosive blast mild traumatic brain injury. Handbook of Clinical Neurology 127, 309–318.

Jensen, J.H., Helpern, J.A., Ramani, A., Lu, H., Kaczynski, K., 2005. Diffusional kurtosis imaging: the quantification of non-gaussian water diffusion by means of magnetic resonance imaging. Magnetic Resonance in Medicine: An Official Journal of the International Society for Magnetic Resonance in Medicine 53, 1432–1440.

Jezzard, P., Balaban, R.S., 1995. Correction for geometric distortion in echo planar images from b0 field variations. Magnetic resonance in medicine 34, 65–73.

Jones, D.K., Basser, P.J., 2004. "squashing peanuts and smashing pumpkins": how noise distorts diffusion-weighted mr data. Magnetic Resonance in Medicine: An Official Journal of the International Society for Magnetic Resonance in Medicine 52, 979–993.

Kim, S., Kwon, H.J., Kang, E.J., Kim, D.W., 2020. Diffusion-tensor tractography of the auditory neural pathway: clinical usefulness in patients with unilateral sensorineural hearing loss. Clinical Neuroradiology 30, 115–122.

Klein, S., Staring, M., Murphy, K., Viergever, M.A., Pluim, J.P., 2009. Elastix: a toolbox for intensity-based medical image registration. IEEE transactions on medical imaging 29, 196–205.

Kurtcan, S., Alkan, A., Kilicarslan, R., Bakan, A.A., Toprak, H., Aralasmak, A., Aksoy, F., Koçer, A., 2016. Auditory pathway features determined by dti in subjects with unilateral acoustic neuroma. Clinical neuroradiology 26, 439–444.

Leemans, A., Jeurissen, B., Sijbers, J., Jones, D.K., 2009. Exploredti: a graphical toolbox for processing, analyzing, and visualizing diffusion mr data, in: Proc Intl Soc Mag Reson Med, p. 3537.

Leemans, A., Jones, D.K., 2009. The b-matrix must be rotated when correcting for subject motion in dti data. Magnetic Resonance in Medicine: An Official Journal of the International Society for Magnetic Resonance in Medicine 61, 1336–1349.

Lutz, J., Hemminger, F., Stahl, R., Dietrich, O., Hempel, M., Reiser, M., Jäger, L., 2007. Evidence of subcortical and cortical aging of the acoustic pathway: a diffusion tensor imaging (dti) study. Academic radiology 14, 692–700.

Matloff, W.J., Matloff, D.J., Toga, A.W., Cheon, T., Gwak, J., Kim, Y., Park, H.J., Kim, H., 2021. Semi-automated 3d cochlea subregional segmentation on t2-weighted mri scans, in: Proc. Intl. Soc. Mag. Reson. Med, p. 3738.

Møller, A.R., 2011. Anatomy and physiology of the auditory system. Textbook of tinnitus , 51–68.

Pajevic, S., Pierpaoli, C., 1999. Color schemes to represent the orientation of anisotropic tissues from diffusion tensor data: application to white matter fiber tract mapping in the human brain. Magnetic Resonance in Medicine: An Official Journal of the International Society for Magnetic Resonance in Medicine 42, 526–540.

Pierpaoli, C., 2010. Artifacts in diffusion mri. Diffusion MRI: theory, methods and applications , 303–318.

Rosenkrantz, A.B., Padhani, A.R., Chenevert, T.L., Koh, D.M., De Keyzer, F., Taouli, B., Le Bihan, D., 2015. Body diffusion kurtosis imaging: basic principles, applications, and considerations for clinical practice. Journal of Magnetic Resonance Imaging 42, 1190–1202.

Spoendlin, H., 1975. Retrograde degeneration of the cochlear nerve. Acta oto-laryngologica 79, 266–275.

Spoendlin, H., 1985. Anatomy of cochlear innervation. American journal of otolaryngology 6, 453–467.

Spoendlin, H., Schrott, A., 1989. Analysis of the human auditory nerve. Hearing research 43, 25–38.

Steven, A.J., Zhuo, J., Melhem, E.R., 2014. Diffusion kurtosis imaging: an emerging technique for evaluating the microstructural environment of the brain. American journal of roentgenology 202, W26–W33.

Tax, C.M., Bastiani, M., Veraart, J., Garyfallidis, E., Irfanoglu, M.O., 2022. What's new and what's next in diffusion mri preprocessing. NeuroImage 249, 118830.

Tax, C.M., Otte, W.M., Viergever, M.A., Dijkhuizen, R.M., Leemans, A., 2015. Rekindle: robust extraction of kurtosis indices with linear estimation. Magnetic resonance in medicine 73, 794–808.

Tax, C.M., Vos, S.B., Leemans, A., 2016. Checking and correcting dti data. Diffusion Tensor Imaging: A Practical Handbook , 127–150.

Veraart, J., Novikov, D.S., Christiaens, D., Ades-Aron, B., Sijbers, J., Fieremans, E., 2016. Denoising of diffusion mri using random matrix theory. Neuroimage 142, 394–406.

Vos, S.B., Haakma, W., Versnel, H., Froeling, M., Speleman, L., Dik, P., Viergever, M.A., Leemans, A., Grolman, W., 2015. Diffusion tensor imaging of the auditory nerve in patients with long-term single-sided deafness. Hearing Research 323, 1–8. URL: https://www.sciencedirect.com/science/article/pii/S0378595515000209, doi:https://doi.org/10.1016/j.heares.2015.01.010.

Vos, S.B., Jones, D.K., Viergever, M.A., Leemans, A., 2011. Partial volume effect as a hidden covariate in dti analyses. Neuroimage 55, 1566–1576.

Vos, S.B., Tax, C.M., Luijten, P.R., Ourselin, S., Leemans, A., Froeling, M., 2017. The importance of correcting for signal drift in diffusion mri. Magnetic resonance in medicine 77, 285–299.

Wu, C.M., Ng, S.H., Wang, J.J., Liu, T.C., 2009. Diffusion tensor imaging of the subcortical auditory tract in subjects with congenital cochlear nerve deficiency. American journal of neuroradiology 30, 1773–1777.

Yushkevich, P.A., Piven, J., Cody Hazlett, H., Gimpel Smith, R., Ho, S., Gee, J.C., Gerig, G., 2006. User-guided 3D active contour segmentation of anatomical structures: Significantly improved efficiency and reliability. Neuroimage 31, 1116–1128.